

Combined plasmonic gratings in organic solar cells

Honghui Shen^{1,*} and Bjorn Maes^{1,2}

¹Photonics Research Group (INTEC), Ghent University-IMEC, Sint-Pietersnieuwstraat 41, B-9000 Gent, Belgium

²Micro- and Nanophotonic Materials Group, University of Mons, Faculty of Science, Avenue Maistriau 19, B-7000 Mons, Belgium

*honghui.shen@intec.ugent.be

Abstract: We propose an organic solar cell structure with combined silver gratings consisting of both a front and a back grating. This combination provides multiple, semi-independent enhancement mechanisms which act additively, so that a broadband absorption is obtained. Both gratings couple the incident light into various plasmonic modes, showing a more localized or propagating character respectively. In addition, some modes only appear for tilted incident light, and therefore present a complex angle-dependent behavior. We provide extensive numerical simulations, resulting in an optimized period of 490nm, with front grating elements of 60 by 10nm and back elements of 60 by 30nm. With these parameters an integrated absorption enhancement factor around 1.35 is observed, with absorption increasing from 48% to 65% under TM polarized light. In addition, the solar cell with combined gratings is much less sensitive to the angle of incident light than the single grating cases. Furthermore, the grating structure does not have a large influence on the TE polarized light absorption.

© 2011 Optical Society of America

OCIS codes: (350.6050) Solar energy; (240.6680) Surface plasmons; (040.5350) Photovoltaic; (250.5403) Plasmonics; (050.2770) Gratings.

References and links

1. H. Hoppe and N. S. Sariciftci, "Organic solar cells: An overview," *J. Mater. Res.* **19**, 1924–1945 (2004).
2. P. E. Shaw, A. Ruseckas, and I. D. W. Samuel, "Exciton diffusion measurements in poly(3-hexylthiophene)," *Adv. Mater.* **20**, 3516–3520 (2008).
3. G. Yu, J. Gao, J. C. Hummelen, F. Wudl, and A. J. Heeger, "Polymer photovoltaic cells: enhanced efficiencies via a network of internal donor-acceptor heterojunctions," *Science* **270**, 1789–1791 (1995).
4. G. Li, V. Shrotriya, J. Huang, Y. Yao, T. Moriarty, K. Emery, and Y. Yang, "High-efficiency solution processable polymer photovoltaic cells by self-organization of polymer blends," *Nat. Mater.* **4**(11), 864–868 (2005).
5. W. Ma, C. Yang, X. Gong, K. Lee, and A. J. Heeger, "Thermally stable, efficient polymer solar cells with nanoscale control of the interpenetrating network morphology," *Adv. Funct. Mater.* **15**(10), 1617–1622 (2005).
6. Y. Kim, S. Cook, S. M. Tuladhar, S. A. Choulis, J. Nelson, J. R. Durrant, D. D. C. Bradley, M. Giles, I. McCulloch, C.-S. Ha, and M. Ree, "A strong regioregularity effect in self-organizing conjugated polymer films and high-efficiency polythiophene:fullerene solar cells," *Nat. Mater.* **5**(3), 197–203 (2006).
7. S. H. Park, A. Roy, S. Beaupré, S. Cho, N. Coates, J. S. Moon, D. Moses, M. Leclerc, K. Lee, and A. J. Heeger, "Bulk heterojunction solar cells with internal quantum efficiency approaching 100%," *Nat. Photonics* **3**, 207–302 (2009).
8. M. A. Green, K. Emery, Y. Hishikawa, and W. Warta, "Solar cell efficiency tables (version 36)," *Prog. Photovoltaics Res. Appl.* **18**, 144–150 (2010).
9. J. R. Tumbleston, D.-H. Ko, E. T. Samulski, and R. Lopez, "Absorption and quasiguide mode analysis of organic solar cells with photonic crystal photoactive layers," *Opt. Express* **14**, 7670–7681 (2009).

10. Y. Park, E. Drouard, O. El Daif, X. Letartre, P. Viktorovitch, A. Fave, A. Kaminski, M. Lemiti, and C. Seassal, "Absorption enhancement using photonic crystals for silicon thin film solar cells," *Opt. Express* **17**, 14312–14321 (2009).
11. A. J. Morfa, K. L. Rowlen, T. H. Reilly III, M. J. Romero, and J. van de Lagemaat, "Plasmon-enhanced solar energy conversion in organic bulk heterojunction photovoltaics," *Appl. Phys. Lett.* **92**(1), 013504 (2008).
12. F. Chen, J. Wu, C. Lee, Y. Hong, C. Kuo, and M. H. Huang, "Plasmonic-enhanced polymer photovoltaic devices incorporating solution-processable metal nanoparticles," *Appl. Phys. Lett.* **95**(1), 013305 (2009).
13. H. Shen, P. Bienstman, and B. Maes, "Plasmonic absorption enhancement in organic solar cells with thin active layers," *J. Appl. Phys.* **106**(7), 073109 (2009).
14. D. Duche, P. Torchio, L. Escoubas, F. Monestier, J.-J. Simon, F. Flory, and G. Mathian, "Improving light absorption in organic solar cells by plasmonic contribution," *Sol. Energy Mater. Sol. Cells* **93**(8), 1377–1382 (2009).
15. H. A. Atwater and A. Polman, "Plasmonics for improved photovoltaic devices," *Nat. Mater.* **9**(3), 205–213 (2010).
16. I. Diukman, L. Tzabari, N. Berkovitch, N. Tessler, and M. Orenstein, "Controlling absorption enhancement in organic photovoltaic cells by patterning Au nano disks within the active layer," *Opt. Express* **19**(S1), A64–A71 (2011).
17. D. H. Wang, D. Y. Kim, K. W. Choi, J. H. Seo, S. H. Im, J. H. Park, O. O. Park, and A. J. Heeger, "Enhancement of donor-acceptor polymer bulk heterojunction solar cell power conversion efficiencies by addition of Au nanoparticles," *Angew. Chem. Int. Ed.* **50**, 5519–5523 (2011).
18. Y. A. Akimov and W. S. Koh, "Design of plasmonic nanoparticles for efficient subwavelength light trapping in thin-film solar cells," *Plasmonics* **6**(1), 155–161 (2010).
19. V. E. Ferry, L. A. Sweatlock, D. Pacifici, and H. A. Atwater, "Plasmonic nanostructure design for efficient light coupling into solar cells," *Nano Lett.* **8**, 4391–4397 (2008).
20. V. E. Ferry, M. A. Verschuuren, H. B. T. Li, R. E. I. Schropp, H. A. Atwater, and A. Polman, "Improved red-response in thin film a-Si:H solar cells with soft-imprinted plasmonic back reflectors," *Appl. Phys. Lett.* **95**, 183503 (2009).
21. V. E. Ferry, M. A. Verschuuren, H. B. T. Li, E. Verhagen, R. J. Walters, R. E. I. Schropp, H. A. Atwater, and A. Polman, "Light trapping in ultrathin plasmonic solar cells," *Opt. Express* **18**(S2), A237–A245 (2010).
22. A. Abass, H. Shen, P. Bienstman, and B. Maes, "Angle insensitive enhancement of organic solar cells using metallic gratings," *J. Appl. Phys.* **109**, 023111 (2011).
23. R. A. Pala, J. White, E. Barnard, J. Liu, and M. L. Brongersma, "Design of plasmonic thin-film solar cells with broadband absorption enhancements," *Adv. Mater.* **21**(34), 3504–3509 (2009).
24. C.-C. Chao, C.-M. Wang, and J.-Y. Chang, "Spatial distribution of absorption in plasmonic thin film solar cells," *Opt. Express* **18**(11), 11763–11771 (2010).
25. M.-G. Kang, T. Xu, H. J. Park, X. Luo, and L. J. Guo, "Efficiency enhancement of organic solar cells using transparent plasmonic Ag nanowire electrodes," *Adv. Mater.* **22**(39), 4378–4383 (2010).
26. C. Min, J. Li, G. Veronis, J.-Y. Lee, S. Fan, and P. Peumans, "Enhancement of optical absorption in thin-film organic solar cells through the excitation of plasmonic modes in metallic gratings," *Appl. Phys. Lett.* **96**(13), 133302 (2010).
27. M. A. Sefunc, A. K. Okyay, and H. V. Demir, "Volumetric plasmonic resonator architecture for thin-film solar cells," *Appl. Phys. Lett.* **98**(9), 093117 (2011).
28. A. Christ, T. Zentgraf, S. G. Tikhodeev, N. A. Gippius, J. Kuhl, and H. Giessen, "Controlling the interaction between localized and delocalized surface plasmon modes: Experiment and numerical calculations," *Phys. Rev. B* **74**, 155435 (2006).
29. P. Nordlander, C. Oubre, E. Prodan, K. Li, and M. I. Stockman, "Plasmon hybridization in nanoparticle dimers," *Nano Lett.* **4**, 899–903 (2004).
30. A. P. Hibbins, W. A. Murray, J. Tyler, S. Wedge, W. L. Barnes, and J. R. Sambles, "Resonant absorption of electromagnetic fields by surface plasmons buried in a multilayered plasmonic nanostructure," *Phys. Rev. B* **74**, 073408 (2006).
31. P. Bermel, C. Luo, L. Zeng, L. C. Kimerling, and J. D. Joannopoulos, "Improving thin-film crystalline silicon solar cell efficiencies with photonic crystals," *Opt. Express* **15**(25), 16986–17000 (2007).
32. J. N. Munday and H. A. Atwater, "Large integrated absorption enhancement in plasmonic solar cells by combining metallic gratings and antireflection coatings," *Nano Lett.* **11**(6), 2195–2201 (2011).
33. Comsol Multiphysics, <http://www.comsol.com>.
34. E. D. Palik, *Handbook of Optical Constants of Solids* (Academic, 1985).
35. W. Barnes, T. Preist, S. Kitson, and J. Sambles, "Physical origin of photonic energy gaps in the propagation of surface plasmons on gratings," *Phys. Rev. B* **54**(9), 6227–6244 (1996).

1. Introduction

Organic solar cells (OSCs) are of great interest in recent years due to their low-cost processing and high-throughput potential [1]. However, compared e.g. with silicon based solar cells the power conversion efficiency is still low. One of the reasons for the low efficiency is the short exciton diffusion length compared to the absorption length, e.g. exciton diffusion and absorption length are less than 10nm [2] and around 100nm respectively in the popular material poly(3-hexylthiophene):(6,6)-phenyl-C61-butyric-acid-methyl ester (P3HT:PCBM). So far the maximum efficiency reported for OSCs based on P3HT:PCBM with bulk heterojunction structure [3] is around 5% [4–6]. Recently, by using new materials, the efficiency is up to around 8% [7, 8]. Enhanced light trapping is another technique to boost the efficiency.

There are various novel structures being proposed to enhance light harvesting in solar cells, e.g. photonic crystals [9, 10], metallic nanoparticles [11–18], periodic metallic gratings [19–27], and so on. Among them metallic based devices have attracted a large interest due to the strong and localized electromagnetic fields existing in these structures, which is a consequence of the excitation of plasmon polaritons. Often, these excitations are divided into localized modes, such as in nanoparticles (Localized Surface Plasmons, LSPs), and propagating modes at interfaces (Surface Plasmon Polaritons, SPPs). In structures with periodic metallic gratings, mixtures of LSPs and SPPs can be excited depending on the period. For small periods ($< 300\text{nm}$), LSPs are mainly the reason for the light harvesting improvement [25–27]. Scattering into SPPs comes into effect for larger grating periods [19, 22, 24]. In addition, the angular dependent dispersion behavior of these plasmonic modes is complex [28]. For example, two different kinds of modes are observed, the so-called bright and dark modes, with symmetric and antisymmetric field distributions respectively [29]. They have been observed numerically [22] and experimentally [28, 30] in some periodic plasmonic nanostructures. Dark modes are not excitable at the standard perpendicular incidence and need an oblique angle, so that optimized light trapping becomes more intricate.

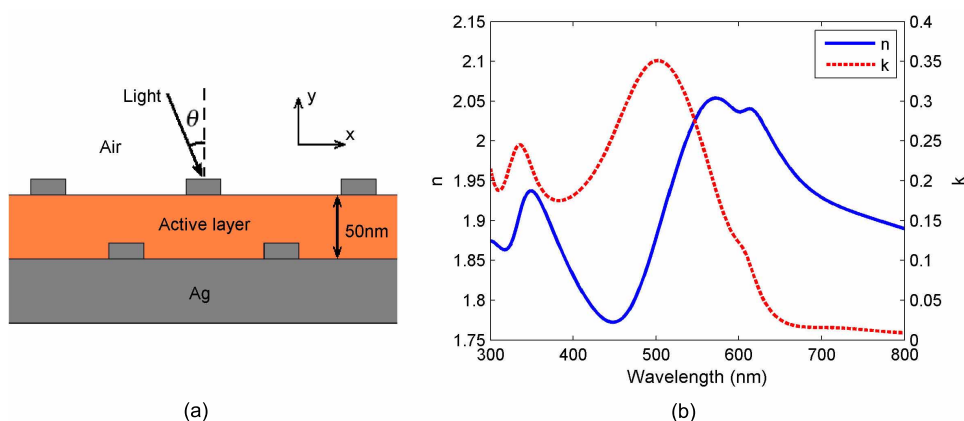


Fig. 1. (a) Schematic diagram of OSCs with combined gratings (front and back grating). (b) Optical constants of P3HT:PCBM with 1:1 weight ratio, n and k are the real and the imaginary parts of the refractive index.

Most previous works focus on how a single nanophotonic feature can enhance the absorption. The study of combined elements to work towards the ultimate light-trapping configuration is less explored [27, 31, 32]. Here we examine the combination of multiple gratings, both on the front and back surface of the absorbing layer, see the model in Fig 1(a). Note that we include a half period offset between the two gratings, so that they operate quasi-independently.

If the elements are on top of each other, thus without offset [27], this leads to different resonances than the individual cases, and can in general give stronger reflections. Remark that our type of offset gratings can naturally form in fabrication processes with conformal layers, and was observed for example in [25]. Thus, here we complement these types of experiments with detailed numerical calculations. Moreover, to better understand the modes we examine the angle-dependent behavior, which is also important for solar cells in practice.

2. Cells with front and back gratings

Throughout our investigations the thickness of the active layer is chosen to be 50nm, corresponding to the first Fabry-Perot maximum for the integrated absorption in a planar reference structure without gratings. Both the excitation of localized modes and Bragg scattering into SPP modes play a role in the grating structures, and are influenced by the dimensions of the front and back grating teeth. Several trade-off mechanisms should be considered. Larger teeth can lead to stronger scattering, but also to more metal absorption. In addition, larger front grating elements augment unwanted reflections, and for the back grating it reduces the amount of available polymer. Sensitive parameters turned out to be the width of the front elements and the height of the back elements. Although not exhaustively optimized, a good value for both widths of 60nm was identified; for the height we employ 10nm for the front, and 30nm for the back grating.

For the numerical calculations we used the finite element method [33] in 2D. The optical constants of P3HT:PCBM are shown in Fig. 1(b). The extinction coefficient k at wavelengths larger than 650nm is mainly caused by PCBM in the blend. Silver data is extracted from [34]. In order to excite plasmonic modes we mainly consider TM polarized light (one H component), at the end of this section we also discuss TE results. Three different types of numerical calculations were carried out. First, to determine the absorption in the active layer we perform a plane wave incidence calculation to model the incoming solar light. In sections 2.1 and 2.2 the calculations correspond to normal incidence; whereas in section 2.3 tilted plane waves are included to determine the angular dependence. Second, to reveal the Bloch modes in the gratings, we perform a Bloch mode analysis with the propagation constant along the x-axis. Finally, for additional information we calculate the dispersion of modes in the planar reference structure, thus without a grating, in order to obtain an initial estimate of possible bandgap locations. To have an overall figure of merit, we calculate the integrated absorption, which integrates the absorption spectrum over the wavelength range from 300 to 800nm weighted by the AM 1.5G solar spectrum.

2.1. Perpendicular incidence absorption spectrum

We consider the optimized period of 490nm (value determined in the next subsection), and examine the absorption in the organic layer for perpendicular TM incidence, see Fig. 2(a). Here the spectrum is indicated for four structures: the planar reference structure without gratings, the front grating case with a flat back surface, the back grating case with a flat air-organic interface, and finally the full combined grating case.

Examining the combined spectra in Fig. 2(a) provides insight in the particular contributions. First, we notice the big peak around 740nm and the shoulder around 600nm in both the front grating and the combined grating case. In contrast, the shoulder of the combined case around 350nm fits well with the back grating absorption. In addition, the small peak around 675nm of the back grating case seems to help the combined case in that range. Thus, the back and the front gratings make fairly independent contributions to different wavelength ranges and one arrives at a broadband enhancement from 350nm to 800nm in the combined grating structure.

The broadband enhancement is attributed to the enhanced field intensity in the vicinity of

gratings due to the excitation of LSPs and SPPs at different wavelengths. To verify this, Fig. 2(b) shows the intensity enhancement in the organic layer in the vicinity of the front and back teeth for combined grating structures. The intensity enhancement is the intensity ratio at a certain point between the cell with a combined grating and the incident field. We notice the strongly enhanced intensity at larger wavelengths ($\lambda > 600\text{nm}$), but the point of largest ratio (near front or back grating) depends on the particular wavelength range.

To better understand the property of the main peak at 740nm, electric E and magnetic H field magnitude distributions are shown in the inset of Fig. 2(a). A mixture between localized (LSP) and propagating (SPP) character is observed [28]. From the H magnitude we indeed see a strong coupling between the front grating element and the back silver interface. From the E magnitude on the other hand we see a strong contribution from the localized excitation of the front element.

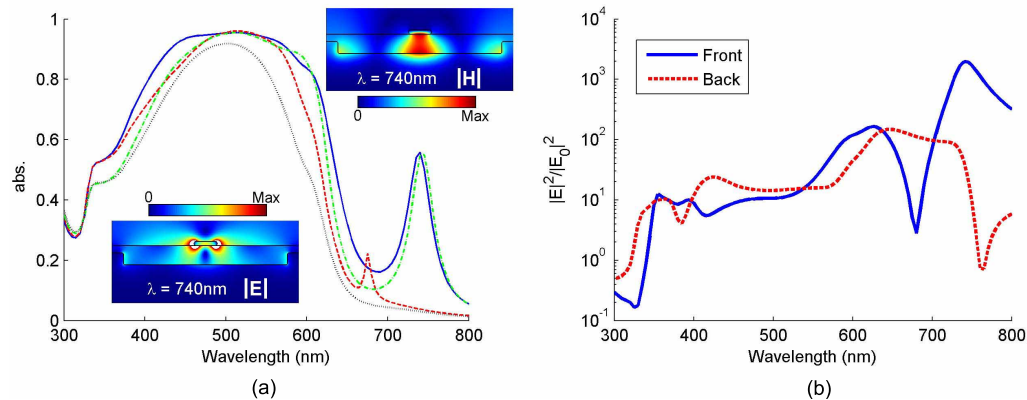


Fig. 2. (a) The absorption spectra of the organic layer with combined grating (blue solid line), front grating only (green dash-dotted), back grating only (red dashed) and planar reference structure without grating (black dotted). The insets show the E and H amplitude profile at wavelength 740nm for the combined case. (b) Intensity enhancement spectrum at a point close to a lower corner of front grating (blue solid line) and at a point close to an upper corner of back grating (red dashed line) for combined grating, normalized by the incident field.

2.2. Period dependence

The period has a strong influence on the grating behavior. Therefore, we consider here the dependence on the period for the combined grating structure, see Fig. 3(a) for normal TM incidence.

For periods larger than 350nm there is an important absorption peak showing up at larger wavelengths ($\lambda > 650\text{nm}$), already discussed in the previous section. This plasmonic resonance red-shifts as the period increases, and finally leaves the absorption tail of the organic material. The strong absorption in the wavelength range 400 to 650nm for periods between 300nm and 600nm is due to more localized grating intensity enhancements, as they are quasi-independent of the period (but more dependent on the grating teeth size, not shown). As the period decreases below 300nm, the filling factor of the gratings gets large, leading e.g. to strongly increased reflection. All of these factors together result in the relatively small absorption in the period range 200–300nm and the wavelength range 400–650nm.

These trends are reflected in Fig. 3(b) for the integrated absorption. At first more light reaches the active layer, leading to a strong absorption increase. After the appearance of the large peak

plasmonic mode a wide optimal plateau (with maximum at 490nm) is reached, after which the mode shifts out of the absorption tail and absorption decreases.

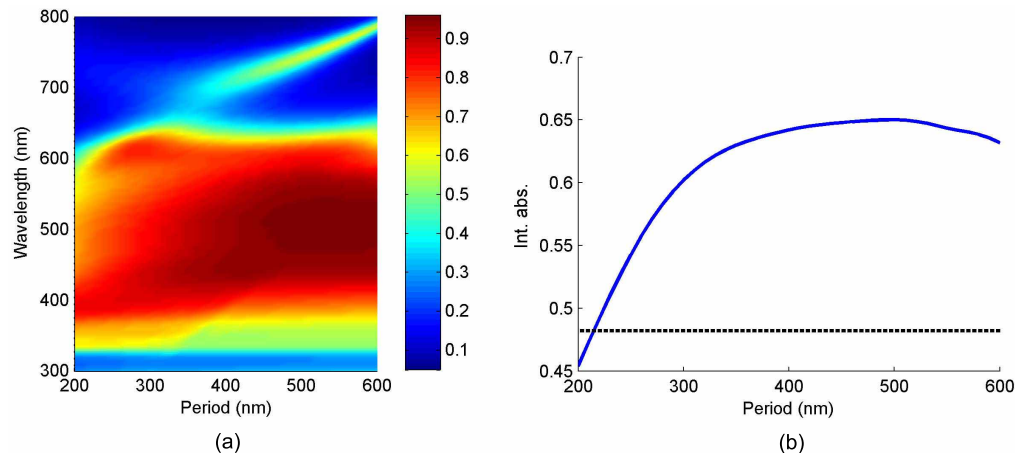


Fig. 3. (a) Map of absorption in the organic layer versus the wavelength of incident light and the grating period. (b) The period dependence of integrated absorption (blue solid line). The value for the reference structure is indicated by the black dotted line.

2.3. Angular dependence

For practical reasons it is important to explore the angular performance of cells with plasmonic gratings. In addition, these studies give insight into the plasmonic modes, and even provide further opportunities for optimization. Fig. 4 maps the absorption in the active layer versus wavelength and light incidence angle for the previously introduced structures: combined, front, back and planar case, respectively.

In Fig. 4(d) we superimpose the folded dispersion of the SPP mode in the planar structure (white dashed line). In addition, we add the folded light line in air (white dash-dotted line). The light line weakly influences the features in Fig. 4(a)–(c), as observed before [35]. The folded SPP dispersion is useful to predict mode (or bandgap) positions at normal incidence when a grating perturbation is introduced. The position of bandgaps around 680nm for the front and back grating case corresponds well, for the combined case the gap has a redshift. In our case the grating perturbation is relatively large, but there is still a decent prediction for the mode bandgaps at perpendicular incidence.

To better understand the properties and splitting of the plasmonic modes we perform Bloch mode calculations with varying propagation constant along the x-axis k_x . We superimpose the dispersion of two Bloch modes on the absorption map in Fig. 4(a)–(c): a bright mode (solid blue line) and a dark mode (dashed red line). We observe very good fits between the Bloch modes and the peaks in the absorption map, although these are different types of calculations, verifying the importance of the Bloch modes for absorption enhancement. We also see that the bright mode in the combined case corresponds well with the front grating case; however, the dark mode of the combined case is shifted. The back grating seems to have a strong influence on the dark mode of the combined case, leading to a very small bandgap. Finally, remark that for each grating structure one of the branches has a flat dispersion curve, indicating a more localized character.

To view the nature of the modes, we plot the H magnitude distribution for Bloch modes at $k_x = 0$ in Fig. 5. The '+' and '-' signs indicate π phase differences in the field profiles.

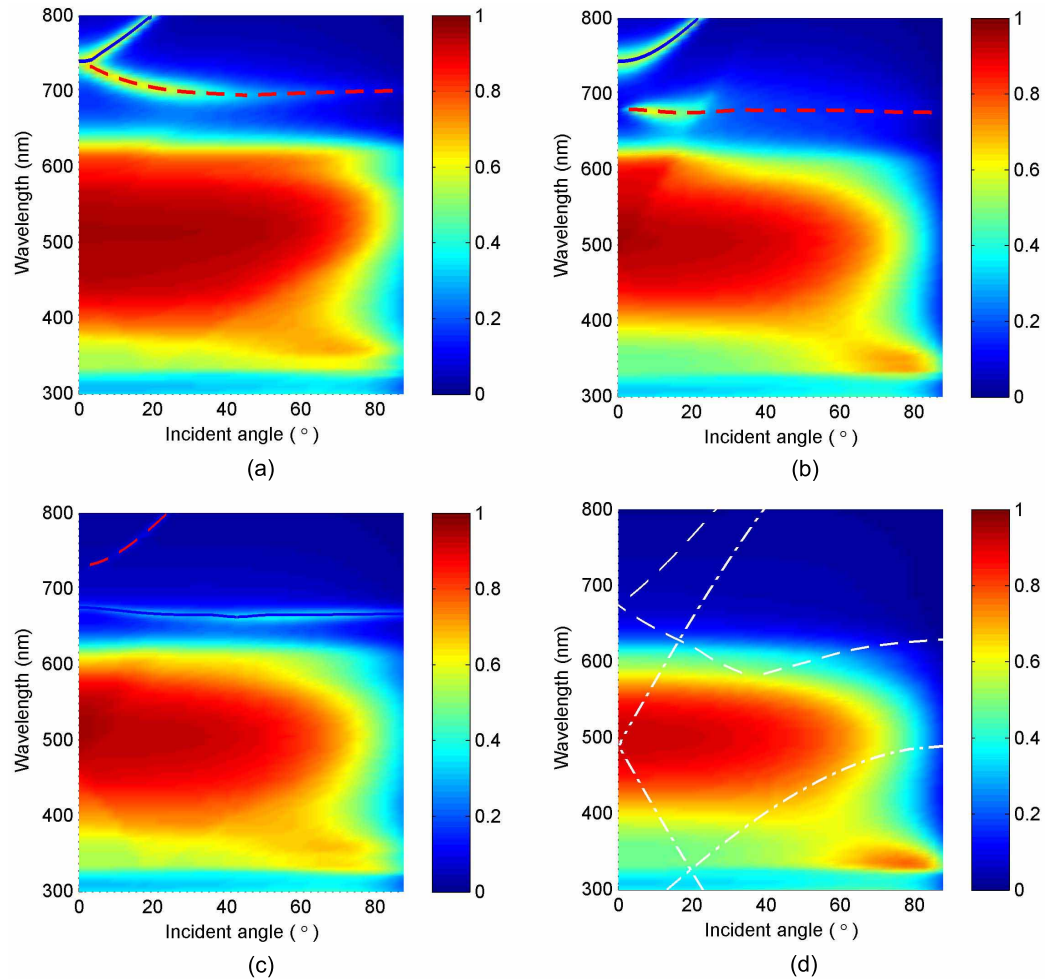


Fig. 4. Angular dependence of absorption with (a) combined grating, (b) front grating, (c) back grating, (d) planar device. Blue solid and red dashed lines superimposed in (a)–(c) are calculated Bloch mode dispersion curves. White dashed and dash-dotted lines in (d) are folded dispersion lines of the planar reference structure (SPP mode) and the folded air light line, respectively.

We observe that the top row (Fig. 5(a), (c), (e)) and the bottom row (Fig. 5(b), (d), (f)) have a different symmetry with respect to the plane in the middle of the structure. This leads to the bright and dark character of the modes, meaning that they can or cannot be excited by perpendicularly incident light, respectively. The symmetry of dark modes leads to a zero overlap with the incoming plane wave, or to a zero net dipole moment [22,29]. The dark mode can only be excited when there is an asymmetry introduced into the system by means of tilting the light incidence or by breaking the symmetry of the geometry. As a consequence, we only observe the dark modes in Fig. 4(a)–(c) for non-perpendicular incidence. Notice that the combined case modes, both bright and dark, look like superpositions of the separate front and back modes, corresponding with the qualitatively similar dispersion curves.

Fig. 6 shows the angular dependence of the integrated absorption. Notice that the integrated absorption for TM reaches its maximum at 10° incidence for the combined grating case, be-

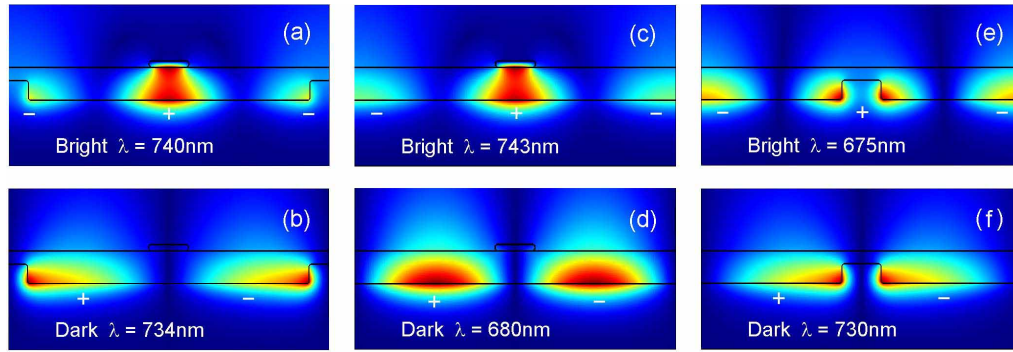


Fig. 5. H field magnitude distribution of Bloch modes. Top row shows bright modes, bottom row are dark modes. (a) and (b) combined grating, (c) and (d) front grating, (e) and (f) back grating case. The '+' and '-' signs denote π phase differences in the field profiles.

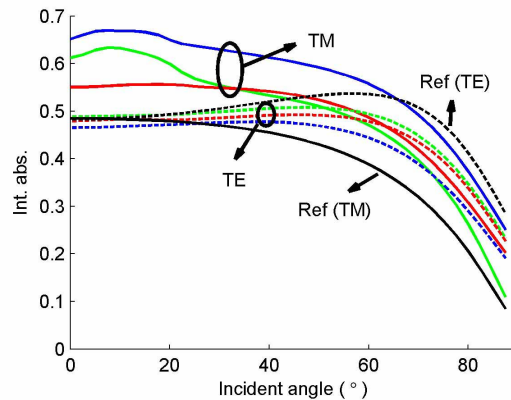


Fig. 6. Integrated absorption versus incidence angle for TM (solid lines) and TE (dashed) polarizations. Blue: combined grating; green: front grating; red: back grating; black: planar structure.

cause of the influence of the dark mode. At normal incidence the combined grating cell reaches around 65%, an enhancement factor of about 1.35 compared with the 48% of a planar cell. The dark mode effect at 10° leads to a further 67% absorption. Enhancement is quite angle insensitive and observed over a large angular range. Up to around 70° the TM absorption is still larger than that of the reference at normal incidence. We can also see that the combined grating case dominates over the front and back single grating cases. Although our structures were mainly optimized for perpendicular incidence, we remark that the dark modes provide an important extra route towards enhancement.

As a final step we should consider the TE polarized and the unpolarized performances, also shown in Fig. 6. For TE it is not possible to excite plasmonic modes, so in this case the silver grating works as absorber and scatterer. Only a very small enhancement near perpendicular incidence for the front grating case is observed. A small decrease of absorption for the back and combined cases is seen for perpendicular incidence, because the presence of the back grating reduces the active material. Considering unpolarized sunlight, the total absorption (abs_{total}) is determined as the average value of absorptions for both TE (abs_{TE}) and TM (abs_{TM}) polarized light, i.e., $abs_{total} = (abs_{TE} + abs_{TM})/2$. As seen in Fig. 6, the absorption enhancement for

TM is much larger than the absorption suppression for TE up to an angle of around 60° . As a result abs_{total} for unpolarized light is still enhanced considerably for a large angular range. For instance for unpolarized perpendicular light, gratings can still enhance the absorption with an average, relatively good enhancement factor of around 1.2.

3. Conclusion

In conclusion, we investigated the influence of combined gratings on the absorption in the active layer of organic solar cells. A broadband absorption enhancement over a large angular range observed. With an optimal period a factor 1.35 enhancement is reached for TM polarized perpendicular light. The enhancements are traced back to modes in the individual front or back grating cases, so the structures function semi-independently. Detailed Bloch dispersion calculations present the mixed character of localized and propagating plasmonic modes, and the bright and dark character. The dark modes provide a mechanism for absorption over a large angular range. Finally, we find that the TE component of the solar light will not decrease the observed enhancement strongly.

Acknowledgments

The authors thank D. Cheyons for P3HT:PCBM measurements and A. Abass for useful discussions. This research was supported by the IWT (Institute for the Promotion of Innovation by Science and Technology in Flanders) via the SBO-project No. 060843 "Polyspec", by the Interuniversity Attraction Poles program of the Belgian Science Policy Office under Grant No. IAP P6-10 "photonics@be" and by COST action MP0702.